NJC

Accepted Manuscript

This is an *Accepted Manuscript*, which has been through the Royal Society of Chemistry peer review process and has been accepted for publication.

Accepted Manuscripts are published online shortly after acceptance, before technical editing, formatting and proof reading. Using this free service, authors can make their results available to the community, in citable form, before we publish the edited article. We will replace this *Accepted Manuscript* with the edited and formatted *Advance Article* as soon as it is available.

You can find more information about *Accepted Manuscripts* in the Information for Authors.

Please note that technical editing may introduce minor changes to the text and/or graphics, which may alter content. The journal's standard Terms & Conditions and the Ethical guidelines still apply. In no event shall the Royal Society of Chemistry be held responsible for any errors or omissions in this *Accepted Manuscript* or any consequences arising from the use of any information it contains.

ROYAL SOCIETY OF CHEMISTRY

www.rsc.org/njc

Ultratrace detection of toxic heavy metal ions found in water bodies using hydroxyapatite supported nanocrystalline ZSM-5 modified electrodes

Balwinder Kaur[a], Rajendra Srivastava*[a], and Biswarup Satpati[b]

[a]*Department of Chemistry, Indian Institute of Technology Ropar, Rupnagar-140001, India*

[b]*Surface Physics and Material Science Division, Saha Institute of Nuclear Physics, 1/AF, Bidhannagar, Kolkata 700 064, India*

E-mail: rajendra@iitrpr.ac.in

Phone: +91-1881-242175; Fax: +91-1881-223395

Abstract

Silver ion-exchanged nanocrystalline ZSM-5 (Ag-Nano-ZSM-5) and ZSM-5 (Ag-ZSM-5) materials were synthesized. Hydroxyapatite supported on zeolite materials were prepared by incubating the Ag ion-exchanged zeolite materials in simulated body fluid at 310 K. The resultant materials were characterized using X-ray diffraction, N_2-adsorption and Scanning/Transmission electron microscopy. Hydroxyapatite supported on Ag ion-exchanged zeolite modified glassy carbon electrodes were fabricated and investigated as electrochemical sensors in the detection of toxic heavy metal ions (Cd^{2+}, Pb^{2+}, As^{3+}, and Hg^{2+}). The results show that the developed sensor exhibited excellent electro-catalytic activity, sensitivity, and stability toward the detection of selected heavy metal ions. The analytical application of the developed sensor is shown in the determination of heavy metal ions found in different water bodies.

Keywords: Nanocrystalline zeolite, hydroxyapatite, nanocomposite, electrochemical sensing, heavy metal ions.

1. Introduction

The contamination of toxic heavy metal ions in water bodies is a serious worldwide threat to human health. Toxic heavy metal ions present in drinking water cause many health problems such as skin lesions, lung cancer, bladder cancer and several other diseases.[1, 2] Therefore, it is important to develop an accurate, fast, and sensitive method to detect and monitor these environmental pollutants. According to World Health Organization (WHO), the allowable level of toxic heavy metals such as Cd^{2+}, Pb^{2+}, As^{3+}, Hg^{2+} in the drinking water is 3 ppb, 10 ppb, 10 ppb, and 6 ppb, respectively.[3] The typical concentration ranges for these heavy metal ions in the real samples vary with source and place. However, the local mineral deposits may produce higher levels in ground water. For example, natural water sources contain much higher levels of arsenic (20-3000 ppb) in the drinking water and the dissolved metal concentrations for cadmium and lead in the Sabarmati River was 0.019 ppb-0.042 ppb and 0.3 ppb-11.65 ppb, respectively.[4, 5]

Atomic absorption spectroscopy (AAS), atomic fluorescence spectrometry, inductively coupled plasma atomic emission spectrometry and inductively coupled plasma mass spectrometry (ICP-MS) can be used for the detection of heavy metal ions.[6-8] The detection limit obtained by these commonly used methods are: Cd^{2+} (0.01 ppb by ICP-MS, 2 ppb by flame AAS), Pb^{2+} (1 ppb by AAS), As^{3+} (0.1 ppb by ICP-MS, 2 ppb by flame AAS), and Hg^{2+} (0.05 ppb by cold vapour AAS, 0.6 ppb by ICP, 5 ppb by flame AAS).[3] But these methods require expensive instruments, high operating cost, and well trained technician to conduct the measurements, which are not suitable for routine on-field monitoring for a large number of samples. Among the common detection techniques, electrochemical methods are the most favoured techniques for the determination of heavy metal ions because of their low cost, high sensitivity, simple operation, accurate determination, rapid analysis time, and portability.[9, 10] Among the different electrochemical methods, electrochemical stripping voltammetric analysis is a very powerful technique for the determination of heavy metal ions. Over the past decades, mercury electrode has been widely used as the working electrode in the determination of heavy metal ions.[11-13] However, the toxicity of mercury and operational limitations restrict its use. Therefore, various mercury free electrodes such as gold electrodes, silver electrodes, boron doped diamond electrodes, glassy carbon electrodes, carbon paste electrodes, and bismuth film electrodes have been developed for the sensitive detection of heavy metal ions.[14-16] But the sensitivity of bulk electrodes does not meet the requirements for the detection of trace heavy

metal ions. Moreover, bulk electrodes are associated with several problems such as a large over potential required for analyte deposition, a high stripping potential needed for analyte detection, the interference of other coexisting metals, and surface fouling. To overcome these problems, chemically modified electrodes have been developed to improve the sensitivity, selectivity, detection limit, and other features of solid electrodes.[17-22] Compared to the traditional solid electrodes, the development of chemically modified electrodes based on nanostructure materials has received significant interest due to their enhanced electrochemical performances because of their large surface area, fast electron transfer rate, and high electro-catalytic activities.[17] The nanostructure material modified electrodes also significantly improve the surface fouling problem associated with the solid electrodes. Although there are many reports available in literature which deals with the determination of heavy metal ions, it is still a challenge to develop a novel, non-toxic, sensitive, and selective electrochemical sensor for the ultra-trace detection of heavy metal ions.[23-28] The objective of this study is to achieve this goal.

Our research is focused on the synthesis of nanocrystalline zeolites and explores their applications in electrocatalysis.[29-34] Though zeolites cover a large industrial catalysis market due to their unique microporous nature and strong acidity,[35, 36] but their application as sensor for large molecules is limited due to microporous nature. Therefore, development of mesoporous zeolites with inter/intra-crystalline mesopores is very important. Efforts have been made to develop soft and hard templates based synthesis strategy to prepare mesoporous zeolites.[37] Our group has also developed several soft-templates based synthesis methodology to prepare nanocrystalline/mesoporous zeolites of different framework structures.[38, 39] In recent years, zeolites have been widely used in the fabrication of electrochemical sensors and biosensors due to their high surface area, porous nature, ion-exchange capacity, and ease of surface functionalization. It has been recently reported by us that nanocrystalline zeolite significantly improves the sensing ability when compared to bulk zeolite material.[29, 32, 34] Further, in recent years, hydroxyapatite (HAP) [$Ca_{10}(PO_4)_6(OH)_2$] modified electrodes have been widely investigated due to their acid base properties, ion-exchange ability, and high adsorption capacity.[40-43] HAP with different morphologies can be prepared using various synthetic routs.[44] However, HAP prepared by these reported methods lacks porosity and high surface area.

In this work, effort was made to combine the advantages of both, HAP and nanocrystalline zeolite materials by incorporating HAP on the surface of zeolite. In this study,

silver ion-exchanged Nano-ZSM-5 (Ag-Nano-ZSM-5) and ZSM-5 (Ag-ZSM-5) materials were prepared. HAP supported on zeolite materials were prepared by incubating in simulated body fluid (SBF). HAP supported zeolite modified glassy carbon electrodes were fabricated and investigated as electrochemical sensors in the detection of toxic heavy metal ions (Cd^{2+}, Pb^{2+}, As^{3+}, and Hg^{2+}) found in water bodies. To the best of our knowledge, this is the first report, which deals with the electrochemical determination of ultra-trace heavy metal ions using HAP supported on Ag-Nano-ZSM-5 as electrode material.

2. Experimental Section

2.1. Materials

All chemicals were of AR grade and used as received without further purification. Tetraethylorthosilicate (TEOS, 98%), tetrapropylammonium hydroxide (TPAOH), and propyltriethoxy silane (PrTES, 97%) were purchased from Sigma Aldrich. Silver nitrate ($AgNO_3$) was obtained from Fisher Scientific. Sodium arsenite ($NaAsO_2$), mercuric chloride ($HgCl_2$), lead acetate ($Pb(CH_3COO)_2$) and cadmium nitrate ($Cd(NO_3)_2.4H_2O$) were purchased from SD Fine Chemical Limited. Tris buffer (tris(hydroxymethyl)aminomethane, $C_4H_{11}NO_3$) was obtained from Sisco Research Laboratories Pvt. Ltd. Sodium hydrogen carbonate ($NaHCO_3$), potassium chloride (KCl), sodium chloride (NaCl), and magnesium chloride hexahydrate ($MgCl_2.6H_2O$) were obtained from Merck. Sodium sulfate (Na_2SO_4) was obtained from Himedia. Deionized water from Millipore Milli-Q system (Resistivity 18 MΩcm) was used in the electrochemical studies. Electrochemical measurements were performed in phosphate buffer (*Sorenson's buffer*) solution that was prepared by mixing NaH_2PO_4 and Na_2HPO_4. The standard phosphate buffer solutions with different pH values (lower or higher) were prepared by adding 0.1 M aqueous H_3PO_4 or NaOH solution to 0.1 M aqueous phosphate buffer solution (PBS), while magnetically stirring until the pH of the aqueous solution reached the desired value.

2.2. Materials synthesis

Nanocrystalline zeolite (Nano-ZSM-5) and conventional zeolite (ZSM-5) were synthesized by following the reported procedure (Supporting Information).[29] Nano-ZSM-5/ZSM-5 (1 g) was

ion-exchanged with 20 mL of 0.1 M $AgNO_3$ aqueous solution at 343 K for 12 h to obtain Ag-Nano-ZSM-5/Ag-ZSM-5.

For the synthesis of HAP supported on zeolite materials, first SBF solution was prepared. SBF solution was prepared in 700 mL of deionized water by adding the reagents in the order of NaCl (6.547 g), $NaHCO_3$ (2.268 g), KCl (0.373 g), Na_2HPO_4 (0.178 g), $MgCl_2.6H_2O$ (0.305 g), $CaCl_2.2H_2O$ (0.368 g), Na_2SO_4 (0.071), and tris buffer (6.057 g). A total of 40 mL of 1 M HCl solution was consumed for pH adjustment during the preparation of SBF solution. 15 mL aliquot of this HCl was added just before addition of sixth reagent ($CaCl_2.2H_2O$). After the addition of eighth reagent (tris buffer), solution temperature was raised to 310 K. 25 mL HCl and remaining water (total volume 1 L) were added slowly to the resultant solution to obtain pH 7.4 at 310 K. The total ionic concentration of SBF prepared is provided in Table S1. 0.2 g of zeolite sample was immersed in 150 mL SBF solution in tightly capped polypropylene bottle and kept in thermostatic bath at 310 K for different periods of time (10 days and 20 days). After completing each immersion period, the samples were washed with deionized water and dried at room temperature for further analysis. HAP supported on Ag-Nano-ZSM-5 and Ag-ZSM-5 samples are designated as HAP/Ag-Nano-ZSM-5 and HAP/ZSM-5, respectively.

For comparative study, conventional hydroxyapatite was prepared by following the reported procedure.[45]

2.3. Instrumentation

X-ray diffraction (XRD) patterns were recorded in the 2θ range of 5-60° with a scan speed of 2°/min on a PANalytical X'PERT PRO diffractometer using Cu Kα radiation (λ=0.1542 nm, 40 kV, 40 mA) and a proportional counter detector. Nitrogen adsorption measurements were performed at 77 K by Quantachrome Instruments, Autosorb-IQ volumetric adsorption analyzer. Sample was out-gassed at 573 K for 3-4 h in the degas port of the adsorption apparatus. The specific surface area of materials was calculated from the adsorption data points obtained at P/P_0 between 0.05-0.3 using the Brunauer-Emmett-Teller (BET) equation. The pore diameter was estimated using the Barret-Joyner-Halenda (BJH) method. Scanning electron microscopy (SEM) measurements were carried out on a JEOL JSM-6610LV, to investigate the morphology of the materials. Transmission electron microscopy (TEM) measurements were carried out using FEI, Tecnai G^2 F30, S-Twin microscope operating at 300 kV. The microscope is equipped with a

high-angle annular dark field (HAADF) detector from Fischione (model 3000) and a scanning unit. The compositional analysis was performed using EDX (EDAX Inc.) attachment in the same microscope. The sample was dispersed in ethanol using ultrasonic bath, and dispersed sample was mounted on a carbon coated Cu grid, dried, and used for TEM measurement.

2.4. Electrode fabrication

Square wave stripping voltammetry (SWSV) studies were performed using Potentiostat-Galvanostat BASi EPSILON, USA. A three electrode electrochemical cell was employed with Ag/AgCl as the reference electrode (3M KCl), HAP/Ag-Nano-ZSM-5 mounted glassy carbon (3 mm diameter) as the working electrode, and Pt foil as the counter electrode. Before modification, the glassy carbon electrode (GCE) was first polished to a mirror like surface with alumina slurry and then ultrasonicated in ethanol and deionized water for 5 min, respectively. 10 µL aliquot of HAP/Ag-Nano-ZSM-5 suspension (a homogenous sonicated solution of 2 mg of HAP/Ag-Nano-ZSM-5, 10 µL of Nafion and 1 mL of deionized water) was placed onto the GCE surface. The electrode was dried in air leaving the material mounted onto the GC surface. For comparison other modified GCE were also prepared using the same process. Electrochemical impedance spectroscopy (EIS) was performed using Autolab PGSTAT302N. Since large amount of HAP nanoparticles were formed on the surface of zeolite after incubating in SBF solution for 20 days, therefore HAP/Ag-Nano-ZSM-5 and other samples with 20 days incubation period in SBF were used in all the electrochemical experiments. Various steps involved in the fabrication of electrochemical sensor are shown in Scheme 1.

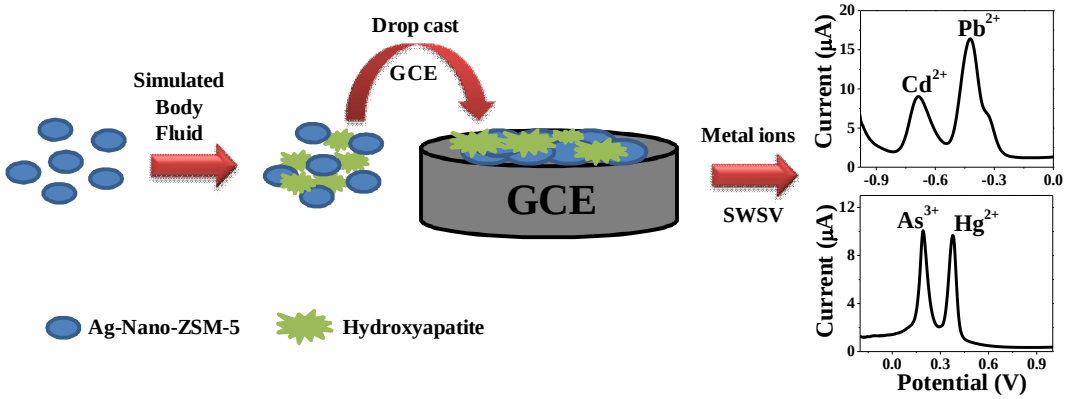

Scheme 1. Schematic depiction for the fabrication of HAP/Ag-Nano-ZSM-5 based sensor.

2.5. Detection of heavy metal ions

Square wave stripping voltammetry (SWSV) was used for the detection of heavy metal ions under optimized conditions. The major steps involved in SWSV were: accumulation of heavy metal ions at an optimized potential and stripping of the accumulated heavy metals. Then the stripping signal corresponding to the concentration of heavy metal ions in solution was monitored. Therefore, first pre-concentration or accumulation of heavy metal ions on HAP/Ag-Nano-ZSM-5/GCE surface was carried out by immersing the electrode into a stirred 0.1 M PBS solution containing the heavy metal ions at an optimized potential for 100 s. After a 15 s resting period, the square wave stripping voltammetry step was carried out in the required potential range in unstirred solution, and the corresponding current signal variance was recorded as a function of potential (Parameters: Step potential 4 mV; square wave amplitude 25 mV; and square wave frequency 15 Hz).

3. Results and Discussion

It is known in the literature that introduction of metal ions or functional groups (such as proteins, dopamine, and peptide/amino acids) promote the formation of HAP in SBF.[46-50] Therefore, in this study, silver ion-exchanged zeolite materials were prepared. Furthermore, it is also known that growth of HAP is facilitated in SBF.[51, 52] The growth process involves the initial nucleation and subsequent growth of HAP from aqueous SBF on the surface of material.[53] In this study, efforts have been made to synthesize HAP nanoparticles in nanocrystalline zeolite matrix by incubating the material in SBF. The details of physico-chemical characterization of the nanocomposite are provided in the following section. HAP/Ag-Nano-ZSM-5 modified glassy carbon electrodes were constructed for the ultra-trace detection of toxic heavy meal ions (Cd^{2+}, Pb^{2+}, As^{3+} and Hg^{2+}).

3.1. Physico-chemical characterizations of the materials

Formation of HAP nanoparticles on various zeolite materials was confirmed using XRD. XRD analysis confirmed that HAP was not formed in the XRD pattern of resultant materials obtained by incubating parent ZSM-5 and Nano-ZSM-5 in SBF solution (Fig. S1). Whereas, HAP was observed in the XRD pattern of resultant materials obtained by incubating Ag-ZSM-5 and Ag-Nano-ZSM-5 in SBF solution (Fig. 1 and Fig. S1). ICP analysis confirmed that large

amount of HAP was formed in Ag-Nano-ZSM-5 matrix when compared to Ag-ZSM-5 (Table 1). These observations confirmed that incorporation of Ag^{+} in the zeolite matrix was required for the formation of HAP. The detailed characterization of HAP/Ag-Nano-ZSM-5 is provided below.

XRD pattern for Ag-Nano-ZSM-5 sample, before and after incubation in SBF with different soaking times is shown in Fig. 1a. Ag-Nano-ZSM-5 exhibited MFI framework structure with high phase purity (Fig. 1a). XRD pattern of Ag-Nano-ZSM-5 is broad in nature, confirming the nanocrystalline nature of the material. The XRD patterns of material recovered after the incubation period of 10 and 20 days show diffraction peaks corresponding to both, Ag-Nano-ZSM-5 and HAP. The characteristic peaks at 25.9°, 27.8°, 32.2°, 32.9°, 34.4°, 38.2°, 46.5°,48.5°, and 49.4° corresponds to the reflection of (002), (102), (112), (300), (202), (310), (222), (312), and (213) planes of HAP (Fig. 1a).[54] The diffraction pattern clearly shows that HAP was formed on Ag-Nano-ZSM-5 matrix by the incubation in SBF. Elemental analysis further confirmed that Ca and P have been incorporated in the samples after incubation in SBF. Analysis confirmed that more amounts of Ca and P were incorporated in the sample, which was incubated for 20 days, when compared to sample obtained after 10 days incubation (Table 1).

The textural properties of the materials were investigated by N_2 adsorption-desorption measurements. The N_2-adsoption isotherm for Ag-Nano-ZSM-5 and HAP/Ag-Nano-ZSM-5 (20 days immersion period) showed a type-IV isotherm similar to the mesoporous materials (Fig. 1b). The major difference in the isotherm of Ag-Nano-ZSM-5 when compared to Ag-ZSM-5 is a distinct increase of N_2-adsorption in the region $0.4<P/Po<0.95$, which is interpreted as capillary condensation in the inter-crystalline mesopore void spaces. The mesopores for Ag-Nano-ZSM-5 and HAP/Ag-Nano-ZSM-5 show a pore size distribution in the range of 2-10 nm. Textural properties of various materials obtained from N_2-adsorption study are summarized in Table 1. N_2-adsorption investigation clearly shows that the total surface area, external surface area and pore volume of Ag-Nano-ZSM-5 is much larger than that of conventional Ag-ZSM-5 (Table 1). Table 1 shows that after the formation of HAP on Ag-Nano-ZSM-5 matrix, total surface area and external surface area was decreased. This indicates that HAP was supported on the external surface of Ag-Nano-ZSM-5, which is responsible for the reduction of external surface area. It may further be noted that total pore volume of Ag-Nano-ZSM-5 and HAP/Ag-Nano-ZSM-5 were almost same, which indicates that the formation of HAP nanocrystals do not plug the mesopores of Ag-Nano-ZSM-5.

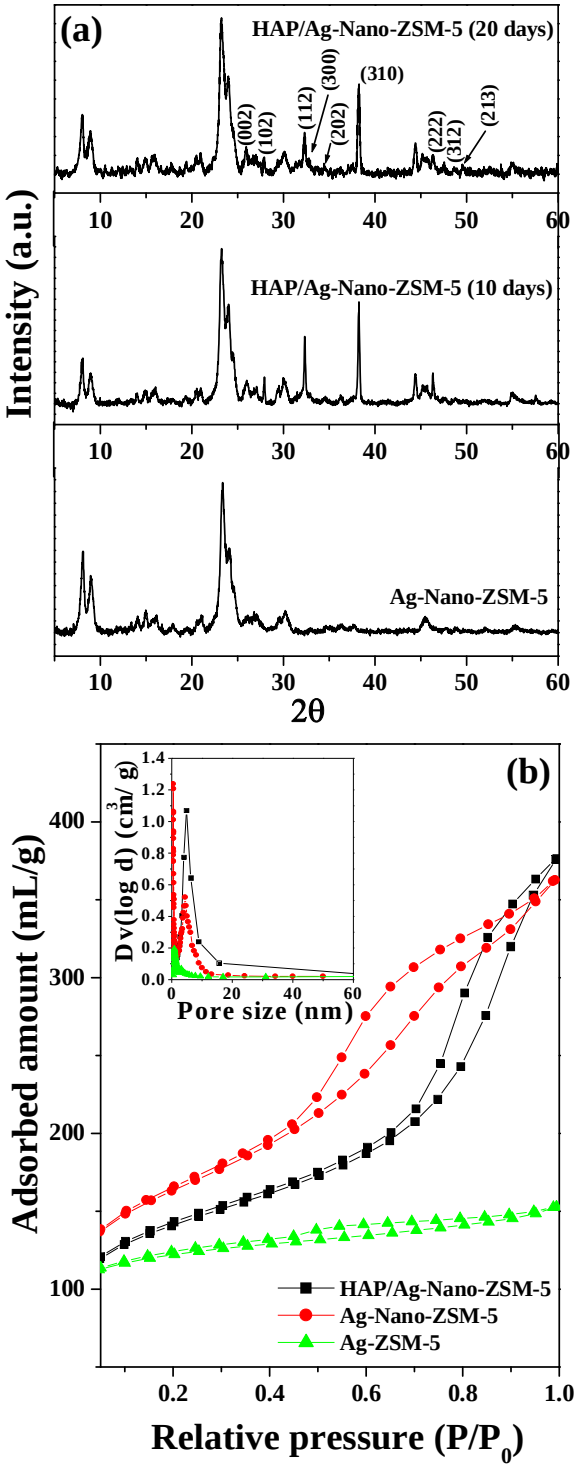

Fig. 1. (a) XRD patterns of Ag-Nano-ZSM-5 before and after the incubation in SBF at different intervals of time (10 days and 20 days), and (b) N_2-adsorption isotherms of Ag-Nano-ZSM-5, HAP/Ag-Nano-ZSM-5 (immersion period 20 days), and Ag-ZSM-5 materials.

Table 1: Physico-chemical characteristics of various materials investigated in this study.

Sample	Ag content (wt %)[c]	Amount of HAP grown in zeolite matrix (wt %)[c]	Total surface area S_{BET} (m^2/g)	External surface area (m^2/g)	Total pore volume (cm^3/g)
HAP/Ag-Nano-ZSM-5[a]	0.96	7.9	462	229	0.52
HAP/Ag-Nano-ZSM-5[b]	0.98	5.4	501	296	0.55
HAP/Ag-ZSM-5[a]	0.98	2.1	267	20	0.19
Ag-Nano-ZSM-5	1.05	-	542	364	0.58
Ag-ZSM-5	1.02	-	378	63	0.24

[a] Material obtained after the incubation period of 20 days in SBF solution.
[b] Material obtained after the incubation period of 10 days in SBF solution.
[c] Content obtained using ICP analysis.

Fig. 2 shows the SEM images of Ag-Nano-ZSM-5 samples before and after the incubation in SBF for 10 and 20 days. Uniform spherical particles were observed for Ag-Nano-ZSM-5 (Fig. 2a). Formation of HAP particles was observed in the Ag-Nano-ZSM-5 matrix, as shown in the SEM image of sample incubated for 10 days (Fig. 2b). After the incubation period of 20 days, densely packed HAP nanoparticles were formed in Ag-Nano-ZSM-5 matrix (Fig. 2c). EDX analysis was also performed along with SEM. EDX analysis confirmed that more amount of HAP was formed in Ag-Nano-ZSM-5 matrix when compared with Ag-ZSM-5 after 20 days of incubation period (Fig. S2).

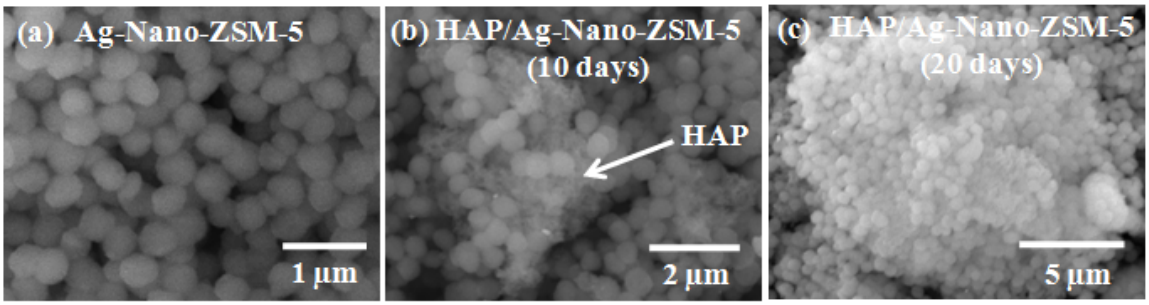

Fig. 2. SEM images of Ag-Nano-ZSM-5 before and after the incubation in SBF at different intervals of time (10 days and 20 days).

TEM was used to investigate the growth and morphology of HAP nanoparticles grown in Ag-Nano-ZSM-5 matrix after incubation period of 20 days in SBF. Fig. 3 clearly shows that the spherical 200-500 nm zeolite particles are made up of 10-20 nm size zeolite particles. High resolution TEM images show that HAP with nanosheet like morphology was grown in Ag-Nano-ZSM-5 matrix. The strong concentric ring in the selected area electron diffraction (SAED) pattern can be indexed as the (002) and (211) diffractions of HAP, displaying its polycrystalline nature (Fig. 3a).

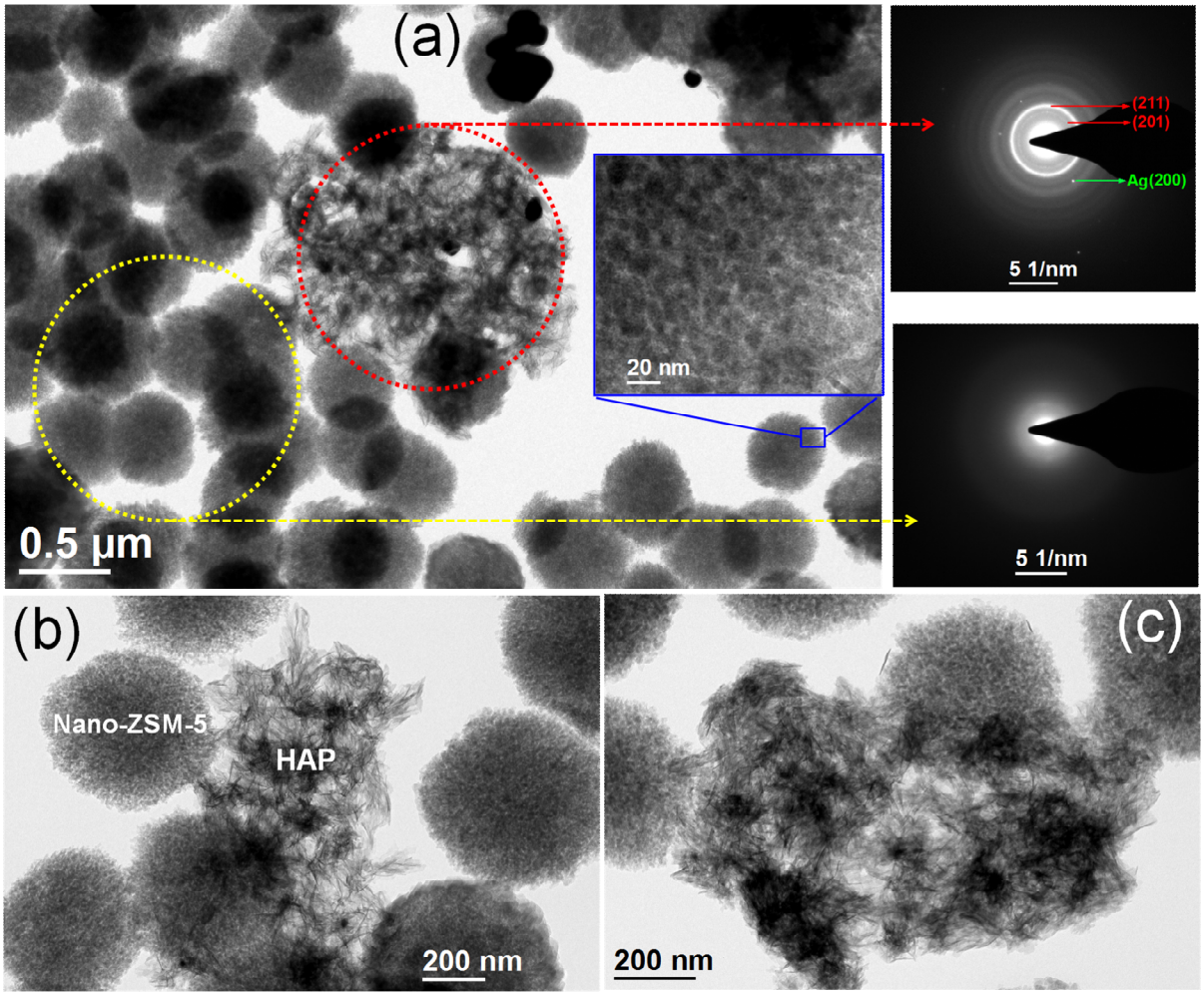

Fig. 3. (a) TEM image of Ag-Nano-ZSM-5 after 20 days incubation in SBF. Arrows indicate SAED patterns from dotted circles. Inset showing magnified image of zeolite particles and (b-c) Magnified images showing how HAP is attached with Nano-ZSM-5.

To investigate the chemical composition of the HAP and surrounding matrix, HAADF analysis was performed (Fig. 4a). The EDX spectrum confirms the presence of Ca, P, Ag, Si, Al, Na, and O, which further confirmed the growth of HAP in Ag-Nano-ZSM-5 matrix (Fig. 4b). It may be noted that C signals observed in the EDX mapping are due to the carbon-coated grid used in the analysis. For a detailed distribution of atomic content inside the nanocrystals, elemental mapping of Si, O, Al, Ca, P, and Ag was performed using drift corrected EDX spectrum imaging using STEM-HAADF mode. The STEM-HAADF image and the corresponding chemical maps for Si, O, Al, Ca, P, and Ag from the marked area 1 in Fig. 4c are

presented in the inset of Fig. 4c and Fig. 4d, respectively. EDX maps confirmed the anchoring between Ag-Nano-ZSM-5 and HAP.

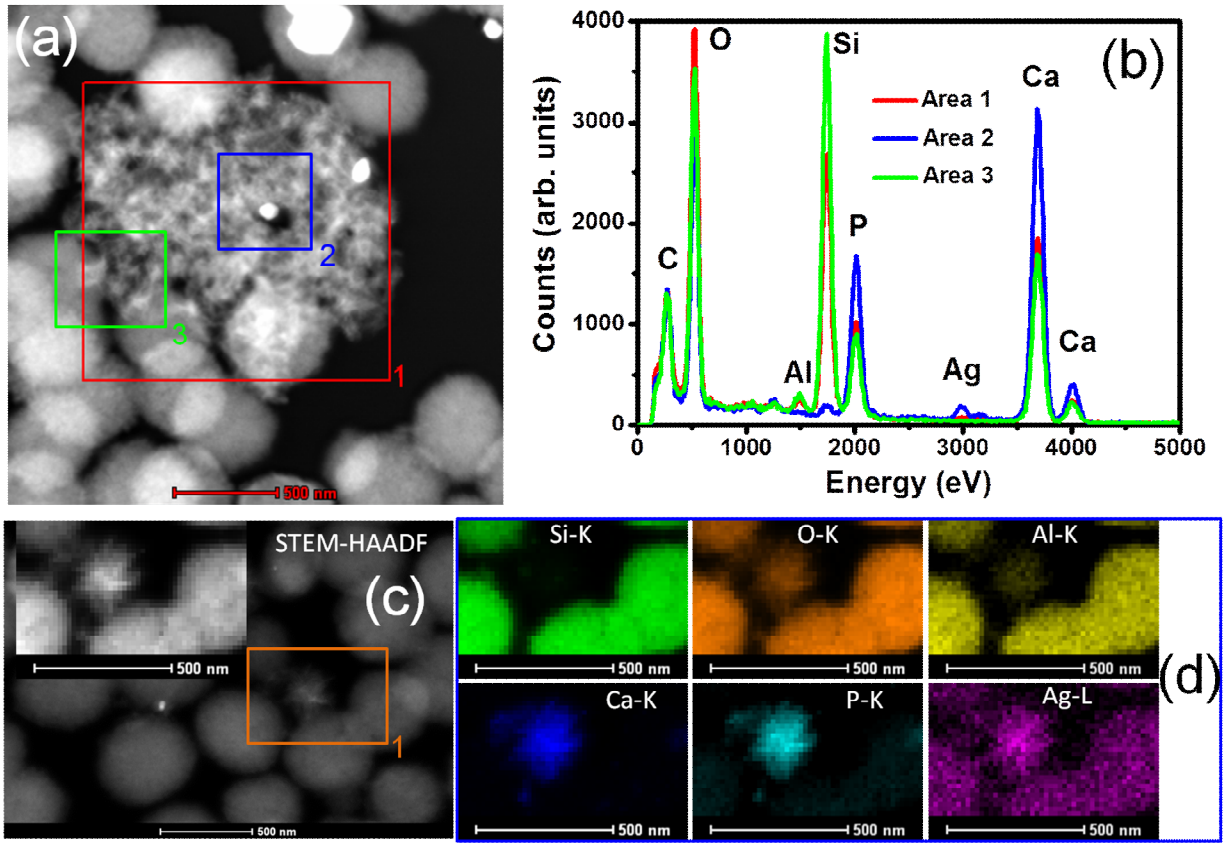

Fig. 4. (a) Scanning TEM-HAADF image of Ag-Nano-ZSM-5 after 20 days incubation in SBF, (b) EDX spectra from different area marked in (a), (c) STEM-HAADF image of HAP/Ag-Nano-ZSM-5 and (d) chemical maps of the representative elements in HAP/Ag-Nano-ZSM-5 from rectangular area marked in (c).

Based on above analysis results, mechanism for the formation of HAP in Ag-Nano-ZSM-5 matrix is proposed. Ag-Nano-ZSM-5 exhibits large external surface area and possesses large number of surface silanol groups. Large number of external surface silanol groups and ion-exchange sites help in the adsorption of calcium and phosphate ions from the SBF in Ag-Nano-ZSM-5. Ag^{+} present in the zeolite matrix accelerates the nucleation and growth of HAP nanoparticles. It may be noted here that no HAP was formed on Nano-ZSM-5, which clearly shows that Ag^{+} is responsible for nucleation and growth of HAP. Small surface area and

significantly less number of surface silanol groups are responsible for the growth of lower amount of HAP in Ag-ZSM-5 matrix. The motive of growing HAP nanoparticles on nanocrystalline zeolite is to use them as body implant materials in bone healing process. In-depth biochemical studies are underway, which will be communicated later.

3.2. Electrochemical characterization of modified electrodes

EIS was employed to characterize the interface properties of the modified electrodes. EIS was carried out in 0.1 M KCl solution containing 10 mM $K_3[Fe(CN)_6]/K_4[Fe(CN)_6]$ over a frequency range of 0.1 Hz to 10^5 Hz with the AC signal amplitude of 5 mV (Fig. 5). In a typical Nyquist plot, the semicircle portion corresponds to the electron-transfer resistance (R_{et}) at higher frequency range whereas a linear part at lower frequency range represents the diffusion limited process.[55] Fig. 5 shows that bare GCE exhibited a large semicircle portion indicating a high electron transfer resistance. Nano-ZSM-5/GCE and ZSM-5/GCE both exhibited reduced semicircular domain and linear portion indicating the mixed charge transfer and diffusion kinetics controlled reactions. The modification of GCE with Ag-Nano-ZSM-5 and HAP/Ag-Nano-ZSM-5 displayed an almost straight line, suggesting the promotion of electron transfer process at the modified electrode surface. Therefore, the presence of Ag^+ ions in the zeolite matrix enhanced the electron transport at the modified electrode surface. Hence, Ag-Nano-ZSM-5/GCE and HAP/Ag-Nano-ZSM-5/GCE significantly facilitates the electron transfer rate and improves the diffusion of ferricyanide towards the electrode interface. Therefore, owing to the fact that Ag-Nano-ZSM-5 has least electron transfer resistance and HAP has good adsorbing ability towards heavy metal ions, HAP/Ag-Nano-ZSM-5/GCE was then employed for the electrochemical determination of selected heavy metal ions.

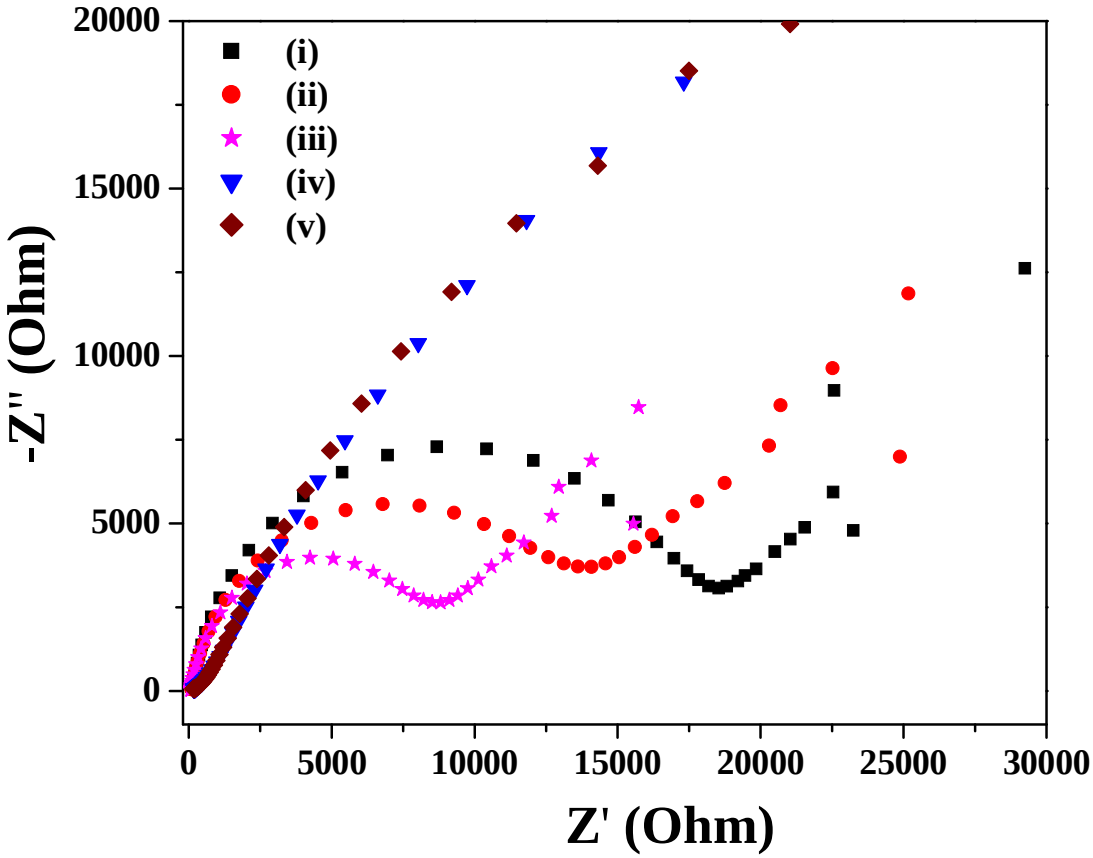

Fig. 5. Nyquist plots of impedance spectra at (i) bare GCE, (ii) ZSM-5/GCE, (iii) Nano-ZSM-5/GCE, (iv) Ag-Nano-ZSM-5/GCE, and (v) HAP/Ag-Nano-ZSM-5/GCE in 0.1 M KCl solution containing 10 mM $[Fe(CN)6]^{3-/4-}$ over the frequency range from 0.1 Hz to 10^5 Hz.

3.3. Optimization of experimental conditions

Square wave stripping voltammetry (SWSV) was used for the detection of heavy metal ions (Cd^{2+}, Pb^{2+}, and Hg^{2+}). Cd^{2+}, Pb^{2+}, and Hg^{2+} were deposited at the optimized potential by the reduction of Cd^{2+}, Pb^{2+}, and Hg^{2+} in 0.1 M PBS solution containing the selected heavy metal ions at HAP/Ag-Nano-ZSM-5/GCE surface. Then the square wave stripping voltammetry step (reoxidation of metal to metal ions) of electrodeposited metal was carried out in the required potential range. It may be noted that the predominant arsenite species in water at pH 6 is H_3AsO_3, whereas at pH 7 to 9, it exists as a mixture of H_3AsO_3 (99-35 %) and $H_2AsO_3^-$ (1-65 %).[56, 57] Therefore, the electrochemical detection mechanism of As^{3+} is different from Pb^{2+}, Cd^{2+}, and Hg^{2+}. In the recent years, natural zeolite has been used for the adsorption and removal of

arsenic species from the ground water with high efficiency.[4, 58] The electrochemical behavior of As^{3+} was first investigated using CV in 0.1 M PBS (pH 7) at a scan rate 20 mV/s by scanning between 0.7 V and -0.3 V at HAP/Ag-Nano-ZSM-5/GCE. The CV showed a reduction peak at 0.08 V corresponding to the reduction of As^{3+} to As^{0} and an oxidation peak at 0.150 V corresponding to the oxidation of As^{3+} to As^{0} (Fig. S3). The CV results matches well with the literature report for arsenic detection.[59] SWSV was then used for the detection of arsenic species under optimized conditions. The first step is pre-concentration of arsenic species at HAP/Ag-Nano-ZSM-5/GCE surface from the bulk solution under magnetic stirring. The second step involves the reduction of arsenic species to As^{0} at -0.5 V followed by its stripping (reoxidation of As^{0} to As^{3+}) in a potential range of -0.3 to 1.0 V.[24] In order to get the maximum sensitivity for the detection of heavy metal ions with HAP/Ag-Nano-ZSM-5/GCE, the important parameters (effect of supporting electrolyte, pH of supporting electrolyte, deposition potential, and deposition time) were optimized in the solution containing 50 ppb each of Cd^{2+}, Pb^{2+}, As^{3+}, and Hg^{2+}, individually.

The metal ions have different electrochemical behavior in different electrolytes. The effect of supporting electrolytes NaCl, NaOH, acetate buffer solution (NaAc-HAc) and phosphate buffer solution (NaH_2PO_4-Na_2HPO_4) on stripping peak currents of Cd^{2+}, Pb^{2+}, As^{3+}, and Hg^{2+} were studied. The results showed that Cd^{2+}, Pb^{2+}, As^{3+}, and Hg^{2+} have the best electrochemical responses in 0.1 M phosphate buffer solution (PBS). When the measurements were performed in 0.1 M PBS, the largest stripping peak current, the lowest background current and the well defined voltammetric peaks were obtained. Hence, 0.1 M PBS was employed in further experiments.

The voltammetric behavior of heavy metal ions was strongly influenced by the pH of supporting electrolyte and thus it was essential to select a proper pH value. The effect of pH on the voltammetric response was investigated in a pH range 4 to 8 in 0.1 M PBS. Fig. S4a shows that the peak current for both Cd^{2+} and Pb^{2+} increased with the increase in pH reaching a maximum at pH 5.0, and then decreased again with further increase in pH of buffer solution. In strong acidic conditions, HAP can slowly dissolve and thus loses its ability to immobilize metal ions causing less stripping current. At pH higher than 5, the precipitation of Cd^{2+} and Pb^{2+} was occurred. The decrease of the stripping signal at pH higher than 6 may be related with the hydrolysis of $Cd^{2+}$and Pb^{2+}. Thus, pH 5 in 0.1 M PBS was selected for stripping measurements

of Cd^{2+} and Pb^{2+}. In the case of As^{3+} and Hg^{2+}, maximum peak current was obtained at pH 7. At pH higher than 7, the hydrolysis of As^{3+} and Hg^{2+} took place and thus peak current was found to decrease in the basic medium. Hence, pH 7 was selected as an optimum pH for As^{3+} and Hg^{2+} detection.

To achieve the best sensitivity, suitable deposition potential is very important in stripping analysis. The effect of deposition potential on the peak current of various analytes was studied in the potential range from -1.1 to 0 V. Fig. S4b shows that the maximum stripping peak current was obtained at deposition potential -1.0 V for Cd^{2+} and Pb^{2+}. Applying more negative potentials to HAP/Ag-Nano-ZSM-5/GCE may result in the generation of hydrogen gas which can block the accumulation of analytes from bulk solution onto the electrode surface and hence lowering the peak current.[60] When the deposition potential was more positive, stripping current further decreased. This may be due to the incomplete reduction of Cd^{2+} and Pb^{2+} on HAP/Ag-Nano-ZSM-5/GCE surface, which decreased the stripping peak current.[61] In case of As^{3+} and Hg^{2+}, the maximum stripping peak current was obtained at deposition potential -0.5 V and therefore, it was selected as optimum deposition potential for As^{3+} and Hg^{2+}. The difference observed for different analytes stripping peak currents may be attributed to their different standard potentials.

The deposition time is another important factor that affects the detection limit and sensitivity. Fig. S4c shows that with increase in deposition time from 10 to 100 s, the stripping peak current increased for all the analytes. This increase in the peak current was due to the increased amount of analytes on the modified electrode surface. Although increase in the deposition time improves the sensitivity but it lowers the upper detection limit due to the surface saturation at high metal ion concentrations.[62] Therefore, to achieve good sensitivity, lower detection limit and wide linear range response, 100 s was chosen as the optimum deposition time for all the experiments.

3.4. Electrochemical detection of heavy metal ions

SWSV technique is known to be the most sensitive electroanalysis technique, since it greatly reduces background noise.[63] Therefore, under the optimum experimental conditions, SWSV was used for the electrochemical detection of Cd^{2+}, Pb^{2+}, As^{3+}, and Hg^{2+} at HAP/Ag-Nano-ZSM-5/GCE.

Fig. 6 shows the SWSV for the individual electrochemical detection of Cd^{2+}, Pb^{2+}, As^{3+}, and Hg^{2+} at HAP/Ag-Nano-ZSM-5/GCE at different concentrations. The results show that Cd^{2+}, Pb^{2+}, As^{3+}, and Hg^{2+} can be detected at potentials -0.698, -0.472, 0.180, and 0.379 V respectively, with well defined and distinguishable sharp stripping peaks at HAP/Ag-Nano-ZSM-5/GCE individually. With increase in the concentration of analytes in the electrochemical cell, the stripping peak current increased significantly. A linear dynamic range was obtained from 0.2-1800 ppb for Cd^{2+} (R^2= 0.9984) (Fig. 6a), 0.4-1800 ppb for Pb^{2+} (R^2= 0.9998) (Fig. 6b), 0.8-2000 ppb for As^{3+} (R^2= 0.9996) (Fig. 6c), and 0.7-2000 ppb for Hg^{2+} (R^2= 0.9990) (Fig. 6d). The results indicate that HAP/Ag-Nano-ZSM-5 provides an excellent platform for the detection of selected toxic heavy metal ions.

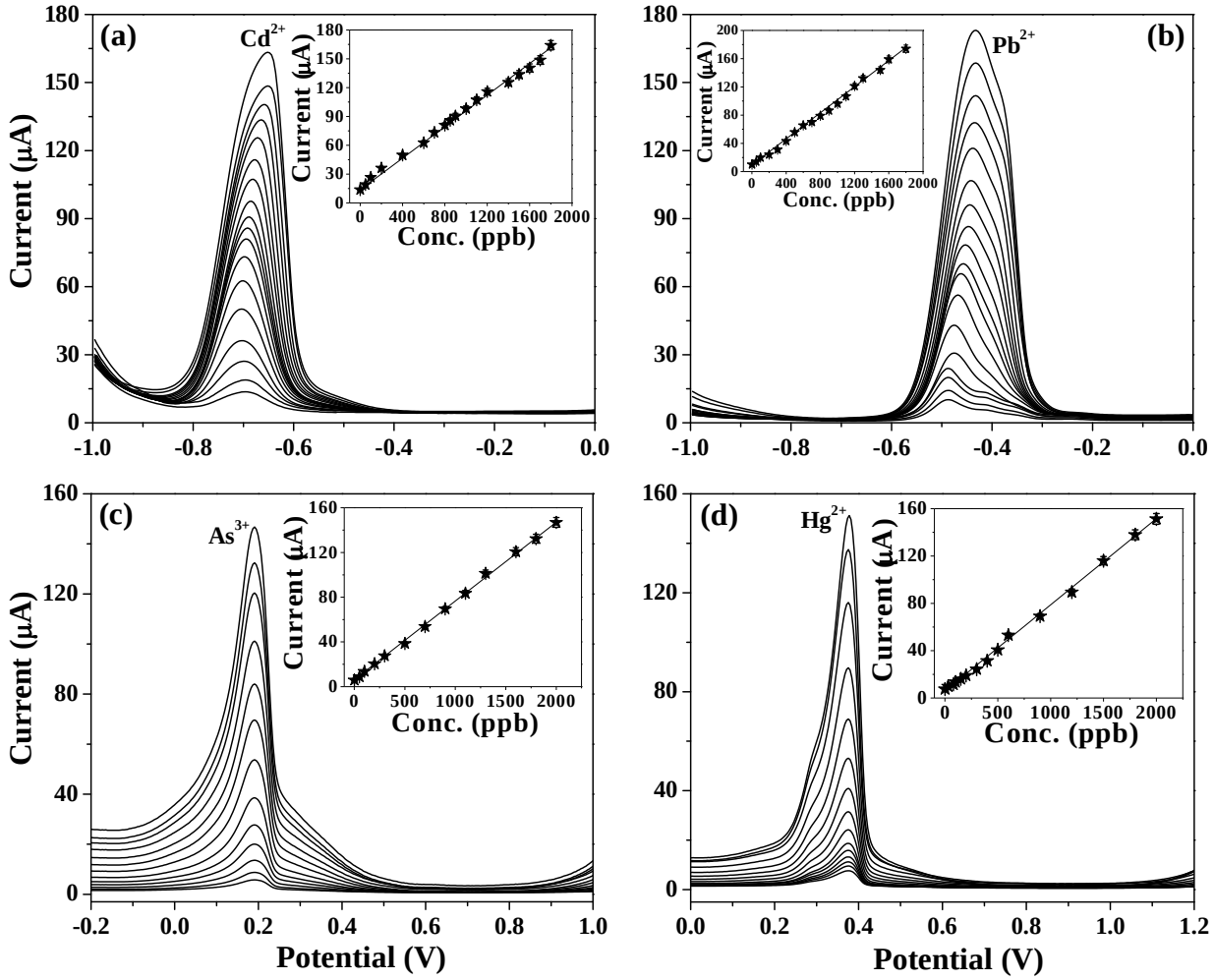

Fig. 6. SWSV at HAP/Ag-Nano-ZSM-5/GCE with different concentrations from inner to outer of curves (a) Cd^{2+} (0.2, 10, 100, 200, 400, 600, 700, 800, 850, 900, 1000, 1100, 1200, 1400, 1500, 1600, 1700, 1800 ppb); (b) Pb^{2+} (0.4, 10, 100, 200, 300, 400, 500, 600, 700, 800, 900, 1000, 1100, 1200, 1300, 1500, 1600, 1800 ppb) in 0.1 M PBS (pH 5) applying deposition potential -1 V and (c) As^{3+} (0.8, 10, 100, 200, 400, 500, 700, 900, 1100, 1300, 1600, 1800, 2000 ppb); (d), Hg^{2+} (0.7, 30, 80, 100, 150, 200, 300, 400, 500, 600, 900,1200, 1500, 1800, 2000 ppb) in 0.1 M PBS (pH 7) applying deposition potential -0.5 V. SWSV parameters were selected as: Step potential 4 mV, square wave amplitude 25 mV, square wave frequency 15 Hz and deposition time 100 s. Inset shows the calibration plot.

Fig. 7a shows the SWSV for the simultaneous electrochemical determination of Cd^{2+} and Pb^{2+} at HAP/Ag-Nano-ZSM-5/GCE by varying their concentrations in 0.1 M PBS (pH 5). Two distinguished and sharp stripping peaks at potentials -0.698 and -0.472 V were obtained during the SWSV experiment containing a mixture of Cd^{2+} and Pb^{2+} at HAP/Ag-Nano-ZSM-5/GCE. The voltammograms for the binary mixture were well separated from each other with a potential difference of $\Delta E_{Cd^{2+}-Pb^{2+}}$ = 226 mV, which was large enough for the simultaneous determination of these analytes in their binary mixture. With increase in the concentration of these analytes in their binary mixture, an enhancement in the stripping peak current was observed. The current obtained was proportional to the concentration of these analytes in their mixture. The peak current obtained was found to be linearly dependent on the concentration in the range of 0.5-1600 ppb for Cd^{2+} (R^2= 0.9992) and 0.6-1600 ppb for Pb^{2+} (R^2= 0.9989). A lower detection limit (S/N=3) of 0.1 ppb and the sensitivity of 1.03 and 1.34 µA/ ppb cm^2 was obtained for Cd^{2+} and Pb^{2+}, respectively. In the similar way As^{3+} and Hg^{2+} were determined simultaneously at HAP/Ag-Nano-ZSM-5/GCE. The voltammetric peaks for the stripping of As^{3+} and Hg^{2+} appeared at 0.188 and 0.379 V in 0.1 M PBS (pH 7) at HAP/Ag-Nano-ZSM-5/GCE with a potential difference of $\Delta E_{As^{3+}-Hg^{2+}}$ = 191 mV. A wide linear range was obtained from 0.9-1800 ppb for As^{3+} (R^2= 0.9996) and 0.8-1800 ppb for Hg^{2+} (R^2= 0.9997). The detection limit (S/N=3) of 0.2 ppb and a sensitivity of 1.08 and 1.04 µA/ ppb cm^2 were obtained for As^{3+} and Hg^{2+}, respectively. However, it may be noted that the detection limits can further be improved by increasing the deposition time. The lower detection limits obtained using HAP/Ag-Nano-ZSM-5/GCE is below the allowable limits instituted by the United States Environmental Protection Agency (EPA) and World Health Organization (WHO).[3] Thus, HAP/Ag-Nano-ZSM-5 nanocomposite can be used as a promising electrode material in the electrochemical detection of selected heavy metal ions with good sensitivity. It was also found that HAP/Ag-Nano-ZSM-5/GCE can be used repeatedly without regenerating or reactivating the surface between successive determinations and can be used for a very long total experimental time.

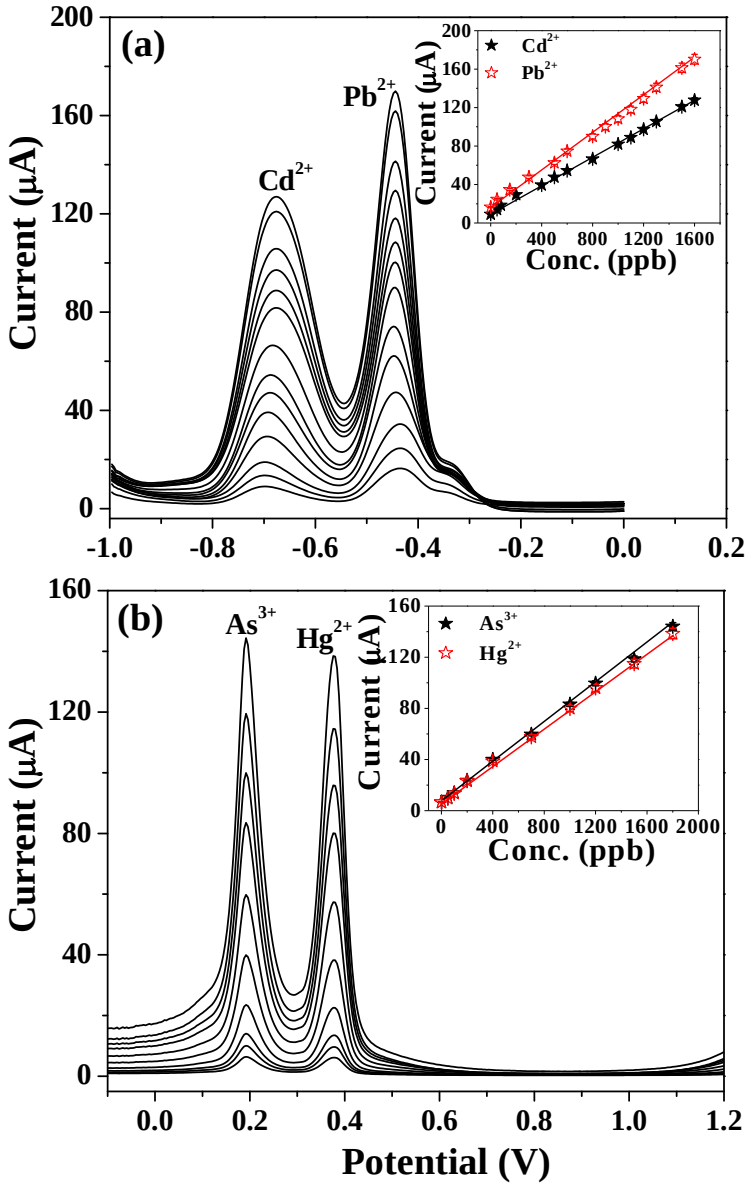

Fig. 7. SWSV at HAP/Ag-Nano-ZSM-5/GCE in the simultaneous detection by varying concentrations of (a) Cd^{2+}, Pb^{2+} in 0.1 M PBS (pH 5) applying deposition potential -1 V and (b) As^{3+}, Hg^{2+} in 0.1 M PBS (pH 7) applying deposition potential -0.5 V. Concentrations from inner to outer of curves: Cd^{2+} (0.5, 10, 80, 200, 400, 500, 600, 800, 1000, 1100, 1200, 1300, 1500, 1600 ppb); Pb^{2+} (0.6, 10, 150, 300, 500, 600, 800, 900, 1000, 1100, 1200, 1300, 1500, 1600 ppb); As^{3+}(0.9, 10, 100, 200, 400, 700, 1000, 1200, 1500, 1800 ppb); and Hg^{2+} (0.8, 10, 100, 200, 400, 700, 1000, 1200, 1500, 1800 ppb). SWSV parameters were selected as: Step potential 4 mV, square wave amplitude 25 mV, square wave frequency 15 Hz and deposition time 100 s. Inset shows the calibration plot.

A comparison for the electrochemical determination of Cd^{2+}, Pb^{2+}, As^{3+} and Hg^{2+} at different modified GCE (HAP/Ag-Nano-ZSM-5/GCE, Ag-Nano-ZSM-5/GCE, and HAP/Ag-ZSM-5/GCE) and bare GCE is provided in Fig. S5. Among all these electrodes investigated, HAP/Ag-Nano-ZSM-5/GCE exhibited the highest current response with the lowest oxidation potential (decrease in the over potential). HAP/Ag-Nano-ZSM-5/GCE exhibited well separated stripping peaks for the simultaneous detection of Cd^{2+} & Pb^{2+} and As^{3+} & Hg^{2+} than bare GCE. Based on these results, one can conclude that HAP/Ag-Nano-ZSM-5/GCE exhibited superior sensing ability and current sensitivity compared to other modified GCE and bare GCE. The increased stripping current at HAP/Ag-Nano-ZSM-5/GC clearly shows that HAP is necessary for the accumulation of heavy metal ions on the electrode surface and confirms that HAP has good adsorbing ability towards selected heavy metal ions. Thus, the obtained results clearly show that HAP/Ag-Nano-ZSM-5 is a promising material possessing the advantages of both HAP and Ag-Nano-ZSM-5 for the electrochemical detection of heavy metal ions. A comparison of HAP/Ag-Nano-ZSM-5/GCE with physical mixture of HAP and Ag-Nano-ZSM-5 toward the electrochemical determination of Cd^{2+}, Pb^{2+}, As^{3+} and Hg^{2+} is shown in Fig. S6. For this study, conventional HAP (16 mg) was physically mixed with Ag-Nano-ZSM-5 (184 mg) (to obtain 8 wt % physical mixtures) in a mortar and pestle, and then used in the fabrication of modified glassy carbon electrode. The results showed that although the physically mixed HAP and Ag-Nano-ZSM-5 was able to detect heavy metal ions but the current response was found to be very low when compared with HAP/Ag-Nano-ZSM-5/GCE. This result confirms that the formation of HAP on Ag-Nano-ZSM-5 using SBF produced very small size HAP (≈ 10 nm) nanoparticles, which is responsible for the high electro-catalytic activity than bulk HAP deposited on Ag-Nano-ZSM-5. A comparison for the sensitivity at different modified electrodes is provided in Fig. 8.

The remarkable electrochemical response of HAP/Ag-Nano-ZSM-5/GCE in electrochemical detection of selected heavy metal ions can be attributed to (i) high adsorbing ability of HAP nanoparticles, (ii) high surface area of HAP/Ag-Nano-ZSM-5 and HAP nanoparticles provide more active sites for electrochemical reactions, (iii) inter-crystalline mesoporosity in Nano-ZSM-5 provides an efficient transport path for the ions because of the short diffusion length and high porosity, (iv) high electronic conductivity due to Ag^{+} ions present in the matrix of Nano-ZSM-5 that accelerates electron transfer at the electrode/electrolyte interface, and (v) lower electron transfer resistance rate at the modified electrode surface. The

comparison of the results shown in this paper with the published literature is provided in Table S2. This method is able to detect Cd^{2+}, Pb^{2+}, As^{3+}, and Hg^{2+} in a wider linear range with lower detection limit, when compared to the literature reports. Hence, HAP/Ag-Nano-ZSM-5 provides an excellent platform for the sensitive determination of heavy metal ions.

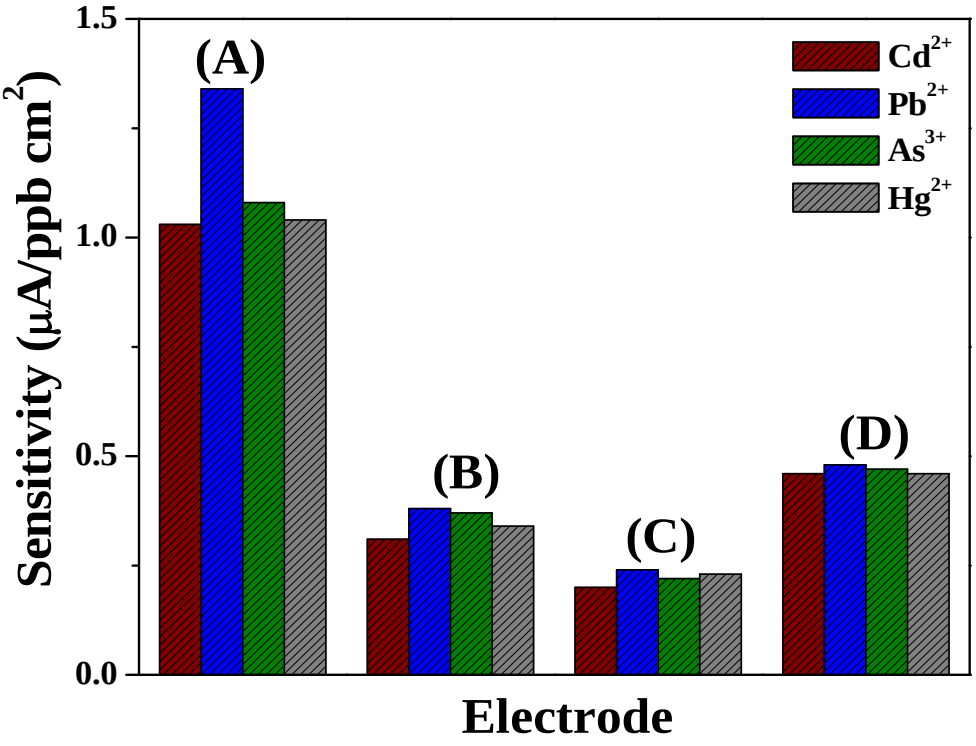

Fig. 8. Comparison of the sensitivity at different modified electrodes (A) HAP/Ag-Nano-ZSM-5/GCE, (B) Ag-Nano-ZSM-5/GCE, (C) HAP/Ag-ZSM-5/GCE, and (D) physically mixed conventional HAP and Ag-Nano-ZSM-5 modified GCE towards the detection of selected heavy metal ions.

3.5. Selectivity, anti-interference, stability and reproducibility of HAP/Ag-Nano-ZSM-5/GCE

Mutual interference is a common problem existing in detection of several metal ions simultaneously. The mutual interference in the simultaneous determination of Cd^{2+} and Pb^{2+} was studied by varying the concentration of one metal ion, whereas the concentration of other metal ion was kept constant in 0.1 M PBS (pH 5) at HAP/Ag-Nano-ZSM-5/GCE (Fig. S7). By keeping the concentration of Pb^{2+} constant but increasing the concentration Cd^{2+}, only the peak current

corresponding to Cd^{2+} increased while the peak current of Pb^{2+} remained constant (Fig. S7a). Similar results were obtained when the concentration of Pb^{2+} was varied whereas the concentration of Cd^{2+} was kept constant (Fig. S7b). In the similar manner, mutual interference was also studied in the simultaneous determination of As^{3+} and Hg^{2+} in 0.1 M PBS (pH 7) (Fig. S7c-d). The results clearly show that no mutual interference among the heavy metal ions was observed in the linear range at HAP/Ag-Nano-ZSM-5/GCE in the detection of the target metal ions, simultaneously. The interference of some foreign substances was also studied to evaluate the selectivity of HAP/Ag-Nano-ZSM-5/GCE in the presence of target heavy metal ions under the optimized conditions. It was observed that common anions (80 fold excess) such as NO_3^-, Cl^-, SO_4^{2-}, PO_4^{3-} and common cations (70 fold excess) such as K^+, Na^+, Mg^{2+}, Ca^{2+}, Al^{3+} had no significant influence on the stripping peak current of Cd^{2+}, Pb^{2+}, As^{3+} and Hg^{2+}.

The interference from other common transition metal ions (such as Zn^{2+} and Cu^{2+}) was also investigated to evaluate the selectivity of HAP/Ag-Nano-ZSM-5/GCE toward the electrochemical detection of Cd^{2+}, Pb^{2+}, As^{3+}, and Hg^{2+}. It may be noted that Zn^{2+} was also detected at -1.13 at HAP/Ag-Nano-ZSM-5/GCE (Fig. S8a). Fig. S8b shows the SWSV response with varying concentrations of Zn^{2+} in the presence of a fixed concentration of Cd^{2+} and Pb^{2+}. The SWSV results show that a 50 fold concentration of Zn^{2+} has no influence on the current response of Cd^{2+} and Pb^{2+}. However, with further increase in concentration of Zn^{2+}, the current response for Cd^{2+} and Pb^{2+} was found to decrease. This may be because of the blockage of active adsorption sites at the electrode surface by Zn^{2+} at this higher concentration. Furthermore, the stripping peak of Zn^{2+} is far away from As^{3+} and Hg^{2+}. Therefore no significant interference was observed in the electrochemical detection of As^{3+} and Hg^{2+} due to Zn^{2+}.

Fig. S9a shows the SWSV response for the individual electrochemical detection of Cu^{2+} at HAP/Ag-Nano-ZSM-5/GCE. The results show that Cu^{2+} exhibits stripping peak at -0.05 V. With increase in concentration of Cu^{2+} in the electrochemical cell the response current was also increased. This implies that the proposed electrode can also be used for the electrochemical detection of Cu^{2+}. Fig. S9b shows the SWSV with varying concentrations of Cu^{2+}, whereas the concentration of Cd^{2+} and Pb^{2+} was kept constant. A 10 fold excess concentration of Cu^{2+} did not show a significant change in the current response of Cd^{2+} and Pb^{2+}. With further increase in the concentrations of Cu^{2+}, the response current of Cd^{2+} and Pb^{2+} was decreased. This decrease in the current response of Cd^{2+} and Pb^{2+} in the presence of high concentrations of Cu^{2+} may be because

of the competition for the limited number of active adsorption sites at the modified electrode surface and the formation of Cu-Cd and Cu-Pb intermetallic compounds.[23, 64, 65] Fig. 10 shows the SWSV with varying concentration of Hg^{2+} in the presence of a fixed concentration of Cd^{2+} and Pb^{2+} at HAP/Ag-Nano-ZSM-5/GCE. The SWSV curve shows that with increase in the concentration of Hg^{2+} in the electrochemical cell, the stripping peak current response corresponding to Cd^{2+} and Pb^{2+} was found to increase. This increase in current response can be explained due to the formation of mercury film at the modified electrode surface. It is reported in literature that Cd^{2+} and Pb^{2+} can be reduced more easily in the presence of Hg^{2+} due to the formation of amalgam.[23, 66] Thus stripping peak response is enhanced in the presence of Hg^{2+} at modified electrode surface.

Fig. S11a shows the influence of Cu^{2+} on the electrochemical detection of As^{3+} at HAP/Ag-Nano-ZSM-5/GCE. The SWSV curve shows that with increase in concentration of Cu^{2+} at a fixed concentration of As^{3+}, the stripping peak current for As^{3+} gradually decreased with a shift in the peak position. Thus Cu^{2+} interfered with the stripping peak for As^{3+}. This interference in the stripping peak for As^{3+} in the presence of Cu^{2+} might be due to the formation of intermetallic compound Cu_3As_2 and competition for the deposition sites at the electrode surface.[24, 67, 68] Fig. S11b shows that a 10 fold excess of Cu^{2+} has no significant interference with the electrochemical detection of Hg^{2+}, whereas with further increase in the Cu^{2+} concentrations, it interfered with the stripping peak current of Hg^{2+}.

To evaluate the stability of HAP/Ag-Nano-ZSM-5/GCE, a series of 20 times repetitive SWSV measurements were performed in the presence of 50 ppb Cd^{2+} under the optimized conditions (Fig. S12). The stripping current of the electrode was highly reproducible with a relative standard deviation (RSD) of 2.24 %. The results showed that HAP/Ag-Nano-ZSM-5/GCE has an excellent stability for repetitive stripping measurements in the experimental conditions. The long term stability of the sensor was evaluated by measuring its sensitivity towards 50 ppb Cd^{2+} for 30 days. The sensor was stored in refrigerator at 298 K and its sensitivity was tested at the interval of 5 days. The SWSV response of the electrode to the same concentration of Cd^{2+} was found to be almost constant with RSD 3.2 %, indicating that the electrode had excellent stability. The reproducibility of the sensor was also evaluated in the sensing studies. Ten HAP/Ag-Nano-ZSM-5/GCEs were made and their current response toward 50 ppb Cd^{2+} was investigated under the optimized experimental conditions (Fig. S13). The

relative standard deviation (RSD) was found to be 3 %, confirming that the fabrication method was highly reproducible.

3.6. Real sample analysis

In order to show the analytical application, the developed sensor was used for the determination of selected heavy metal ions present in different environmental water bodies. The water samples were collected from Sarkhej lake water, Ahmedabad, Gujarat, India and ground water, near Thermal Plant, Bathinda, Punjab, India. Experiments were performed at HAP/Ag-Nano-ZSM-5/GCE to determine the concentration of Cd^{2+}, Pb^{2+}, As^{3+} and Hg^{2+} under the optimized conditions. The content of heavy metal ions was detected using the standard addition method and the results are listed in Table 2. To verify the accuracy of the developed sensor, concentration of metal ions was determined in the real sample using ICP analysis and the results were found in good agreement, confirming that the newly developed sensor is accurate and has promising application in real systems. In order to evaluate the validity of the proposed sensor for the determination of heavy metal ions, recovery studies were carried out using real samples to which known amount of target metal ion was added. The values of recovery were in the range from 98 to 104 %, suggesting the accuracy of HAP/Ag-Nano-ZSM-5/GCE based sensor. These results indicate that the proposed sensor can provide a promising tool for the determination of Cd^{2+}, Pb^{2+}, As^{3+} and Hg^{2+} in environmental water samples with satisfactory recoveries.

Table 2: Determination of Cd^{2+}, Pb^{2+}, As^{3+}, and Hg^{2+} in real samples at HAP/Ag-Nano-ZSM-5/GCE (n = 5).

Real sample analysis without spiking				
Sample	**Analyte**	**Detected by HAP/Ag-Nano-ZSM-5/GCE (ppb)**	**Detected by ICP (ppb)**	**RSD[a] (%)**
Tap Water	Cd^{2+}	ND[b]	ND[b]	-
	Pb^{2+}	ND[b]	ND[b]	-
	As^{3+}	ND[b]	ND[b]	-
	Hg^{2+}	ND[b]	ND[b]	-
Artificial tap water	Cd^{2+}	47.8	51.2	2.6
	Pb^{2+}	51.4	48.9	3.4
	As^{3+}	103.5	102.2	3.8
	Hg^{2+}	99.3	101.8	4.1
Sarkhej lake water, Ahmedabad, Gujarat, India	Cd^{2+}	1398	1402	2.6
	Pb^{2+}	1302	1299	3.8
	As^{3+}	703	701	3.5
	Hg^{2+}	899	903	3.1
Ground water, Thermal Plant, Bathinda, Punjab, India	Cd^{2+}	ND[b]	ND[b]	ND[b]
	Pb^{2+}	20	20.7	2.9
	As^{3+}	1.2	1.5	3.2
	Hg^{2+}	0.5	0.4	3.6

Real sample analysis with spiking					
Sample	**Analyte**	**Original (ppb)**	**Spiking (ppb)**	**Detected (ppb)**	**Recovery (%)**
Artificial tap water	Cd^{2+}	50	100	149	98
	Pb^{2+}	50	100	151	102
	As^{3+}	100	100	204	104
	Hg^{2+}	100	100	197	97
Sarkhej lake water, Ahmedabad, Gujarat, India	Cd^{2+}	1402	50	1465	100.9
	Pb^{2+}	1299	50	1367	101.4
	As^{3+}	701	50	743	98.9
	Hg^{2+}	903	50	959	100.7

[a] Average value of five determinations detected by HAP/Ag-Nano-ZSM-5/GCE, [b] ND = Not detected.

4. Conclusions

Hydroxyapatite nanoparticles supported on silver ion-exchanged nanocrystalline ZSM-5 nanocomposite material was successfully prepared. Physico-chemical characterization reveals that large amount of hydroxyapatite (≈ 8 wt %) with nanosheet morphology was grown in Ag-Nano-ZSM-5 matrix when Ag-Nano-ZSM-5 was incubated in simulated body fluid for 20 days. Electrochemical sensor based on hydroxyapatite nanoparticles supported on silver ion-exchanged zeolite modified glassy carbon electrode was fabricated for the detection of ultra-trace (<1 ppb) amount of toxic heavy metal ions Cd^{2+}, Pb^{2+}, As^{3+} and Hg^{2+}. Among the materials investigated, HAP/Ag-Nano-ZSM-5 exhibited the highest electro-catalytic activity toward the detection of selected heavy metal ions with good stability, sensitivity, and selectivity. High adsorbing ability of hydroxyapatite nanoparticles, high surface area and inter-crystalline mesoporosity of nanocrystalline zeolite and lower electron transfer resistance of nanocomposite material are attributable to its high electro-catalytic activity. Under the optimum conditions, a wide linear range was obtained from 0.5-1600 ppb for Cd^{2+}, 0.6-1600 ppb for Pb^{2+}, 0.9-1800 ppb for As^{3+}, and 0.8-1800 ppb for Hg^{2+}. The detection limit was found to be 0.1, 0.1, 0.2, and 0.2 ppb for Cd^{2+}, Pb^{2+}, As^{3+}, and Hg^{2+}, respectively. The analytical performance of the developed sensor was demonstrated in the detection of these toxic heavy metal ions in different environmental water bodies with satisfactory results.

Acknowledgements

Authors thank Department of Science and Technology, New Delhi for financial assistance (DST grant SB/S1/PC-91/2012). BK is grateful to CSIR, New Delhi for SRF fellowship.

Supporting Information

Electronic Supplementary Information (ESI) available. See DOI

References

1. T. Kemper and S. Sommer, *Environ. Sci. Technol.*, 2002, **36**, 2742-2747.
2. B. K. Mandal and K. T. Suzuki, *Talanta*, 2002, **58**, 201-235.
3. Guidelines for Drinking Water Quality, 4th ed., World Health Organization: Geneva, 2011. http://whqlibdoc.who.int/publications/2011/ 9789241548151_eng.pdf.
4. M. Bilici Baskan and A. Pala, *Desalination*, 2011, **281**, 396-403.
5. T. K. Gandhi, *Global Res. Anal.*, 2013, **2**, ISSN No. 2277-8160.
6. H. Bagheri, A. Afkhami, M. Saber-Tehrani and H. Khoshsafar, *Talanta*, 2012, **97**, 87-95.
7. Y. Li, Y. Jiang, X.-P. Yan and Z.-M. Ni, *Environ. Sci. Technol.*, 2002, **36**, 4886-4891.
8. E. Bulska, M. Wałcerz, W. Jędral and A. Hulanicki, *Anal. Chim. Acta*, 1997, **357**, 133-140.
9. I. Turyan and D. Mandler, *Nature*, 1993, **362**, 703-704.
10. X. Dai, O. Nekrassova, M. E. Hyde and R. G. Compton, *Anal. Chem.*, 2004, **76**, 5924-5929.
11. G. Aragay, A. Puig-Font, M. Cadevall and A. Merkoçi, *J. Phys. Chem. C*, 2010, **114**, 9049-9055.
12. E. Shams, A. Babaei and M. Soltaninezhad, *Anal. Chim. Acta*, 2004, **501**, 119-124.
13. X. Gao, W. Wei, L. Yang, T. Yin and Y. Wang, *Anal. Lett.*, 2005, **38**, 2327-2343.
14. A. Manivannan, M. S. Seehra, D. A. Tryk and A. Fujishima, *Anal. Lett.*, 2002, **35**, 355-368.
15. I. Švancara, C. Prior, S. B. Hočevar and J. Wang, *Electroanalysis*, 2010, **22**, 1405-1420.
16. Y.-C. Sun, J. Mierzwa and M.-H. Yang, *Talanta*, 1997, **44**, 1379-1387.
17. M. Li, H. Gou, I. Al-Ogaidi and N. Wu, *ACS Sustainable Chem. Eng.*, 2013, **1**, 713-723.
18. G. Aragay and A. Merkoçi, *Electrochim. Acta*, 2012, **84**, 49-61.
19. X. Gong, Y. Bi, Y. Zhao, G. Liu and W. Y. Teoh, *RSC Adv.*, 2014, **4**, 24653-24657.
20. R.-X. Xu, X.-Y. Yu, C. Gao, J.-H. Liu, R. G. Compton and X.-J. Huang, *Analyst*, 2013, **138**, 1812-1818.
21. A. Chira, B. Bucur, M. P. Bucur and G. L. Radu, *New J. Chem.*, 2014, **38**, 5641-5646.
22. M. Gich, C. Fernandez-Sanchez, L. C. Cotet, P. Niu and A. Roig, *J. Mater. Chem. A*, 2013, **1**, 11410-11418.

23. C. Gao, X.-Y. Yu, R.-X. Xu, J.-H. Liu and X.-J. Huang, *ACS Appl. Mater. Interfaces*, 2012, **4**, 4672-4682.
24. C. Gao, X.-Y. Yu, S.-Q. Xiong, J.-H. Liu and X.-J. Huang, *Anal. Chem.*, 2013, **85**, 2673-2680.
25. X.-Y. Yu, Q.-Q. Meng, T. Luo, Y. Jia, B. Sun, Q.-X. Li, J.-H. Liu and X.-J. Huang, *Sci. Rep.*, 2013, **3**.
26. X.-Y. Yu, X.-Z. Yao, T. Luo, Y. Jia, J.-H. Liu and X.-J. Huang, *ACS Appl. Mater. Interfaces*, 2014, **6**, 3689-3695.
27. R.-X. Xu, X.-Y. Yu, C. Gao, Y.-J. Jiang, D.-D. Han, J.-H. Liu and X.-J. Huang, *Anal. Chim. Acta*, 2013, **790**, 31-38.
28. X.-Y. Yu, Z.-G. Liu and X.-J. Huang, *Trend Environ. Anal. Chem.*, 2014, **3–4**, 28-35.
29. B. Kaur, M. U. Anu Prathap and R. Srivastava, *ChemPlusChem*, 2012, **77**, 1119-1127.
30. B. Kaur and R. Srivastava, *Electrochim. Acta*, 2014, **133**, 428-439.
31. B. Kaur and R. Srivastava, *Electroanalysis*, 2014, **26**, 1078-1089.
32. B. Kaur and R. Srivastava, *Electroanalysis*, 2014, **26**, 1739-1750.
33. B. Kaur and R. Srivastava, *J. Nanosci. Nanotechnol.*, 2014, **14**, 6539-6550.
34. R. Srivastava, B. Kaur and B. Satpati, *New J. Chem.*, 2014, DOI: 10.1039/C4NJ01360C.
35. A. Corma, *Chem. Rev.*, 1997, **97**, 2373-2420.
36. C. S. Cundy and P. A. Cox, *Chem. Rev.*, 2003, **103**, 663-702.
37. Y. Tao, H. Kanoh, L. Abrams and K. Kaneko, *Chem. Rev.*, 2006, **106**, 896-910.
38. R. Kore, R. Srivastava and B. Satpati, *Chem. Eur. J.*, 2014, **20**, 11511-11521.
39. R. Kore, B. Satpati and R. Srivastava, *Chem. Eur. J.*, 2011, **17**, 14360-14365.
40. Y. Li, X. Liu, X. Zeng, Y. Liu, X. Liu, W. Wei and S. Luo, *Sens. Actuators, B: Chem.*, 2009, **139**, 604-610.
41. Y. Zhang, Y. Liu, X. Ji, C. E. Banks and W. Zhang, *J. Mater. Chem.*, 2011, **21**, 14428-14431.
42. B. Wang, J.-J. Zhang, Z.-Y. Pan, X.-Q. Tao and H.-S. Wang, *Biosens. Bioelectron.*, 2009, **24**, 1141-1145.
43. P. Kanchana, N. Lavanya and C. Sekar, *Mat. Sci. Eng. C*, 2014, **35**, 85-91.
44. Y. Zhang, Y. Liu, X. Ji, C. E. Banks and W. Zhang, *Mater. Lett.*, 2012, **78**, 120-123.

45. Ľ. Medvecký, R. Štulajterová, Ľ. Parilák, J. Trpčevská, J. Ďurišin and S. M. Barinov, *Colloids Surf., A*, 2006, **281**, 221-229.
46. M. C. Bonferoni, G. Cerri, M. de' Gennaro, C. Juliano and C. Caramella, *Appl. Clay Sci.*, 2007, **36**, 95-102.
47. Y. Lin, Z. Yang and J. Cheng, *J. Rare Earth*, 2007, **25**, 452-456.
48. G. Wei, J. Zhang, L. Xie and K. D. Jandt, *Carbon*, 2011, **49**, 2216-2226.
49. C.-Y. Chien, T.-Y. Liu, W.-H. Kuo, M.-J. Wang and W.-B. Tsai, *J. Biomed. Mater. Res. B*, 2013, **101A**, 740-747.
50. J. Ryu, S. H. Ku, M. Lee and C. B. Park, *Soft Matter*, 2011, **7**, 7201-7206.
51. K. Rodríguez, S. Renneckar and P. Gatenholm, *ACS Appl. Mater. Interfaces*, 2011, **3**, 681-689.
52. T. Kokubo, *Biomaterials*, 1991, **12**, 155-163.
53. R. Rajeswari, C. H. N. Clarisse, L. Susan, P. Damian, R. Michael, S. Ramakrishna and K. C. Casey, *Biomed. Mater.*, 2012, **7**, 015001.
54. L. Lao, Y. Wang, Y. Zhu, Y. Zhang and C. Gao, *J. Mater. Sci. - Mater. Med.*, 2011, **22**, 1873-1884.
55. Y. Wei, L.-T. Kong, R. Yang, L. Wang, J.-H. Liu and X.-J. Huang, *Chem. Commun.*, 2011, **47**, 5340-5342.
56. V. M. Boddu, K. Abburi, J. L. Talbott, E. D. Smith and R. Haasch, *Water Res.*, 2008, **42**, 633-642.
57. G. Liu, X. Zhang, J. W. Talley, C. R. Neal and H. Wang, *Water Res.*, 2008, **42**, 2309-2319.
58. M. P. E. Gonzalez, J. Mattusch and R. Wennrich, *J. Environ. Monit.*, 2001, **3**, 22-26.
59. T. Ndlovu, B. B. Mamba, S. Sampath, R. W. Krause and O. A. Arotiba, *Electrochim. Acta*, 2014, **128**, 48-53.
60. Y. Wei, C. Gao, F.-L. Meng, H.-H. Li, L. Wang, J.-H. Liu and X.-J. Huang, *J. Phys. Chem. C*, 2011, **116**, 1034-1041.
61. R. Ouyang, Z. Zhu, C. E. Tatum, J. Q. Chambers and Z.-L. Xue, *J. Electroanal. Chem.*, 2011, **656**, 78-84.
62. X. Gao, W. Wei, L. Yang and M. Guo, *Electroanalysis*, 2006, **18**, 485-492.
63. M. R. Rahman, T. Okajima and T. Ohsaka, *Anal. Chem.*, 2010, **82**, 9169-9176.

64. G. H. Hwang, W. K. Han, J. S. Park and S. G. Kang, *Talanta*, 2008, **76**, 301-308.
65. D. Pan, Y. Wang, Z. Chen, T. Lou and W. Qin, *Anal. Chem.*, 2009, **81**, 5088-5094.
66. H. P. Wu, *Anal. Chem.*, 1996, **68**, 1639-1645.
67. R. Feeney and S. P. Kounaves, *Anal. Chem.*, 2000, **72**, 2222-2228.
68. A. O. Simm, C. E. Banks and R. G. Compton, *Anal. Chem.*, 2004, **76**, 5051-5055.

Figures, Tables and Scheme captions

Figures

Fig. 1 (a) XRD patterns of Ag-Nano-ZSM-5 before and after the incubation in SBF at different intervals of time (10 days and 20 days), and (b) N_2-adsorption isotherms of Ag-Nano-ZSM-5, HAP/Ag-Nano-ZSM-5 (immersion period 20 days), and Ag-ZSM-5 materials.

Fig. 2 SEM images of Ag-Nano-ZSM-5 before and after the incubation in SBF at different soaking time (10 days and 20 days).

Fig. 3 (a) TEM image of Ag-Nano-ZSM-5 after 20 days incubation in SBF. Arrows indicate SAED patterns from dotted circles. Inset showing magnified image of zeolite particles and (b-c) Magnified images showing how HAP is attached with Nano-ZSM-5.

Fig. 4 (a) Scanning TEM-HAADF image of Ag-Nano-ZSM-5 after 20 days incubation in SBF, (b) EDX spectra from different area marked in (a), (c) STEM-HAADF image of HAP/Ag-Nano-ZSM-5 and (d) chemical maps of the representative elements in HAP/Ag-Nano-ZSM-5 from rectangular area marked in (c).

Fig. 5 Nyquist plots of impedance spectra at (i) bare GCE, (ii) ZSM-5/GCE, (iii) Nano-ZSM-5/GCE, (iv) Ag-Nano-ZSM-5/GCE, and (v) HAP/Ag-Nano-ZSM-5/GCE in 0.1 M KCl solution containing 10 mM $[Fe(CN)6]^{3-/4-}$ over the frequency range from 0.1 Hz to 10^5 Hz.

Fig. 6 SWSV at HAP/Ag-Nano-ZSM-5/GCE with different concentrations from inner to outer of curves (a) Cd^{2+} (0.2, 10, 100, 200, 400, 600, 700, 800, 850, 900, 1000, 1100, 1200, 1400, 1500, 1600, 1700, 1800 ppb); (b) Pb^{2+} (0.4, 10, 100, 200, 300, 400, 500, 600, 700, 800, 900, 1000, 1100, 1200, 1300, 1500, 1600, 1800 ppb) in 0.1 M PBS (pH 5) applying deposition potential -1 V and (c) As^{3+} (0.8, 10, 100, 200, 400, 500, 700, 900, 1100, 1300, 1600, 1800, 2000 ppb); (d), Hg^{2+} (0.7, 30, 80, 100, 150, 200, 300, 400, 500, 600, 900,1200, 1500, 1800, 2000 ppb) in 0.1 M PBS (pH 7) applying deposition potential -0.5 V. SWSV parameters were selected as: Step potential 4 mV, square wave amplitude 25 mV, square wave frequency 15 Hz and deposition time 100 s. Inset shows the calibration plot.

Fig. 7 SWSV at HAP/Ag-Nano-ZSM-5/GCE in the simultaneous detection by varying concentrations of (a) Cd^{2+}, Pb^{2+} in 0.1 M PBS (pH 5) applying deposition potential -1 V

and (b) As^{3+}, Hg^{2+} in 0.1 M PBS (pH 7) applying deposition potential -0.5 V. Concentrations from inner to outer of curves: Cd^{2+} (0.5, 10, 80, 200, 400, 500, 600, 800, 1000, 1100, 1200, 1300, 1500, 1600 ppb); Pb^{2+} (0.6, 10, 150, 300, 500, 600, 800, 900, 1000, 1100, 1200, 1300, 1500, 1600 ppb); As^{3+}(0.9, 10, 100, 200, 400, 700, 1000, 1200, 1500, 1800 ppb); and Hg^{2+} (0.8, 10, 100, 200, 400, 700, 1000, 1200, 1500, 1800 ppb). SWSV parameters were selected as: Step potential 4 mV, square wave amplitude 25 mV, square wave frequency 15 Hz and deposition time 100 s. Inset shows the calibration plot.

Fig. 8 Comparison of the sensitivity at different modified electrodes (A) HAP/Ag-Nano-ZSM-5/GCE, (B) Ag-Nano-ZSM-5/GCE, (C) HAP/Ag-ZSM-5/GCE, and (D) physically mixed conventional HAP and Ag-Nano-ZSM-5 modified GCE towards the detection of selected heavy metal ions.

Table

Table 1 Physico-chemical characteristics of various materials investigated in this study.

Table 2 Determination of Cd^{2+}, Pb^{2+}, As^{3+}, and Hg^{2+} in real samples at HAP/Ag-Nano-ZSM-5/GCE (n = 5).

Scheme 1

Scheme 1 Schematic depiction for fabrication of HAP/Ag-Nano-ZSM-5 based sensor.